Production of PHB Scaffolds Reinforced with HAp Through Electrospinning

Tácito Iago Dourado dos Santos[a]* , Alan Christie da Silva Dantas[a], Nelson Cárdenas Olivier[a],

Andre Moreira[a] , Caio Oliveira[b], José Américo de Sousa Moura[c]

[a]*Universidade Federal do Vale do São Francisco, Programa de Pós-Graduação em Ciência dos Materiais (PPGCM), Juazeiro, BA, Brasil.*
[b]*Universidade Federal do Vale do São Francisco, Juazeiro, BA, Brasil.*
[c]*Universidade Federal do Vale do São Francisco, Colegiado de Engenharia Elétrica, Juazeiro, BA, Brasil.*

Electrospinning, an economical technique, is widely used for biomedical scaffold fabrication, crucial in tissue and organ regeneration, particularly with biomaterials. Polymers, either pure or reinforced with ceramics, aid in cell proliferation and tissue formation. Polyhydroxybutyrate (PHB) is a promising biopolymer for tissue engineering, offering biocompatibility comparable to petroleum-derived polymers. Combining PHB with hydroxyapatite (HAp) enhances mechanical strength and osteoconductivity. This study aims to produce electrospun PHB microfibrous webs reinforced with HAp for scaffold fabrication. Morphological variations are analyzed through manipulation of electrospinning parameters. The study observed microfibrous webs with diameters ranging from 2 to 9 µm. Mechanical and microstructural evaluations demonstrate superior strength of PHB/HAp microfibrous webs compared to pure PHB, 1.23 MPa and 0.58 MPa respectively, demonstrating the efficacy of HAp reinforcement. These findings highlight the potential of PHB/HAp microfibrous webs in bone tissue engineering.

Keywords: *Electrospinning, Hydroxyapatite, Polyhydroxybutyrate, Scaffold, Tissue engineering.*

1. Introduction

Among the known methods for obtaining nanofibers, electrospinning has garnered significant attention in the academic world in recent decades. This is evidenced by the substantial increase in publications on the subject, numbering around 2000 articles per year[1]. Electrospinning, known for its simple configuration, has found diverse applications, including filtration[2-4], employment in the textile industry[5-7], catalysis[8-10], tissue engineering[11-13], wound healing[14-16], drug delivery[17-19] and water decontamination[20-22].

Within the various polymeric materials suitable for producing electrified fibers, polyhydroxybutyrate (PHB) has gained attention and extensive study due to its biodegradability, biocompatibility, non-toxicity, and mechanical properties closely resembling those of polymers like polyethylene (PP)[23-25]. However, similar to other organic polymers, PHB has limited bioactivity and is not suitable for applications involving high mechanical stresses. One solution to this challenge involves combining this polyhydroxyalkanoate with a bioceramic to enhance its strength and osteoconductivity compared to the pure polymer[26-28].

Hydroxyapatite (HAp) has demonstrated its potential as a bioceramic that can improve the bioactivity and mechanical properties of PHB[29]. With distinct properties depending on its preparation method, hydroxyapatite is a calcium phosphate compound with the chemical formula $Ca_{10}(PO_4)_6(OH)_2$. This member of the apatite family exhibits properties that render it suitable for various applications, including serving as a synthetic bone substitute, creating extracellular supports/matrixes for tissue engineering involving cytokines, bone, and cartilage cells, and acting as a promoter for improving cell adhesion and dissemination on the surfaces of membranes designed for tissue engineering applications[30-33].

Numerous studies have concentrated on producing PHB/HAp scaffolds for applications in bone tissue engineering, with the aim of achieving bone regeneration at sites affected by damage or injury[29,34]. Other research has investigated the electrospinning of PHB and HAp in combination with polymers like polylactic acid (PLLA)[35] and poly(lactic acid-co-glycolic acid) (PLGA)[36,37].

The electrospinning machine used in this study offers the advantage of cost-effectiveness and ease of replication. This makes it pedagogically suitable and accessible not only for novice researchers in the field of electrospinning but also for research groups operating under budget constraints. Its total cost was US\$172.65, making it intriguing for two key reasons: it competes favorably with similar electrospinning machines developed in contemporary studies focused on the construction and application of such equipment and proves exceptionally cost-effective when compared to commercially available laboratory-grade electrospinning machines (with prices ranging from US\$15,595 to US\$60,000)[38-41].

This study aims to produce microfibrous webs of PHB and PHB/HAp through electrospinning, creating three-dimensional supports/scaffolds. The electrospinning process

*e-mail: tacito.santos@discente.univasf.edu.br

was carried out using a low-cost machine manufactured at the Materials Science Graduate Institute of the Federal University of São Francisco Valley (UNIVASF). Various electrospinning parameters, including solution flow rate, solution concentration, distance between the capillary tube and collector, rotating collector speed, and capillary tube diameter, were adjusted to determine the optimal configuration for fiber production. The effects of these parameters were investigated using scanning electron microscopy (SEM).

2. Materials and Methods

2.1. Electrospinning machine

The electrospinning machine, developed and constructed at the Materials Science Graduate Institute of the Federal University of São Francisco Valley, consists of three essential components: a high-voltage power supply, a controlled injection system (CIS), and a rotating drum collector. The rotating drum is mounted on a mobile base with rails and has a nylon body with its surface covered by an aluminum plate.

A potentiometer is used to control the rotational speed of the drum. The DC motor has a 9V input voltage that can be continuously adjusted from 0 to 9 V, corresponding to an angular velocity ranging from 0 to 580 rpm. The high-voltage source supply in the electrospinning system incorporates a BSC25-0111 106-18G flyback high-voltage transformer and a Huntkey LW-6350HG switched-mode power supply, which together elevate the input voltage from 12 V to 20 kV. The controlled injection system (CIS) consists of a stepper motor coupled to a gear reducer, which, through a spindle, converts the motor's angular motion into linear movement to operate the syringe trigger.

The polymer solution was loaded into 5 mL syringes using needles as capillary tubes. The entire CIS is controlled via Arduino. The developed electrospinning machine had a cost of US$172.65 (approximately R$851,17), as indicated in Table 1. The schematic design of the electrospinning machine can be seen in Figure 1a, while the constructed prototype is depicted in Figure 1b.

2.2. Hydroxyapatite synthesis

Hydroxyapatite was produced following the methodology described by Álvares[42]. The wet precipitation method was employed, utilizing gypsum (calcium sulfate hemihydrate, $CaSO_4.0.5H_2O$) as the calcium source, along with ammonium hydroxide (NH_4OH) and dibasic ammonium phosphate ($(NH_4)_2HPO_4$) as reagents. The molar ratio of Ca/P was calculated to be 1.67 using Equation 1.

$$10CaSO_4.0.5H_2O + 6(NH_4)_2HPO_4 + 8NH_4OH \rightarrow$$
$$Ca_{10}(PO_4)_6(OH)_2 + 10(NH_4)_2SO_4 + 11H_2O \tag{1}$$
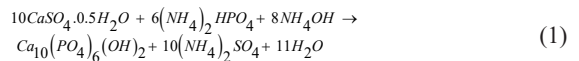
A solution containing 0.2 mol/L of calcium sulfate hemihydrate ($CaSO_4.0.5H_2O$) was continuously stirred while dibasic ammonium phosphate ($(NH_4)_2HPO_4$) at a concentration of 0.12 mol/L was added at a rate of 20 mL/min. The pH of the reaction was controlled and maintained at 9.5 by adding ammonium hydroxide (NH_4OH) at a concentration of 3 mol/L, as needed. After the addition of all reagents, stirring was discontinued, and the solution was allowed to stand for 48 hours. The entire process was carried out at room temperature. After this elapsed time, the solution's pH was adjusted to 7.0 by washing it with deionized water, followed by vacuum filtration of the hydroxyapatite. Subsequently, all the hydroxyapatite was oven-dried for 12 hours at 100 °C. After drying, the material was ground to a fine powder using a mortar and pestle and subjected to calcination for 2 hours at 900 °C.
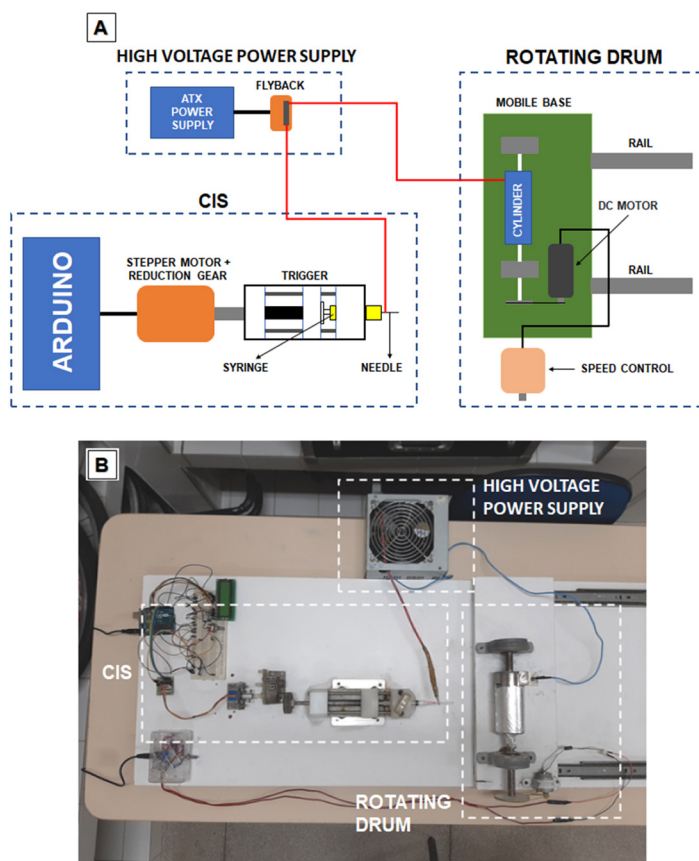
2.3. Polymeric solution

Polymer solutions were prepared using the following materials: PHB powder obtained from PHB Industrial (SP) with a purity exceeding 95% and an average molecular weight of approximately 600,000 g/mol, and chloroform ($CHCl_3$) of PA ACS grade with a purity of 99.8% and a molecular weight of 119.38 g/mol, supplied by Metaquímica. Pure PHB solutions were prepared by magnetic stirring at 3000 rpm while heating to 60 °C for 3 hours until the polymer completely dissolved. PHB/HAp solutions were formulated by adding hydroxyapatite powder, which had been ground and immersed in a chloroform solution in an ultrasonic bath for 30 minutes, to the PHB solution. The mixture was then subjected to magnetic stirring at 3000 rpm and heated to 60 °C for 3 hours until complete dissolution of the polymer.

2.4. Fiber's production

2.4.1. Study of the electrospinning parameters for the production of electrospun PHB and PHB/HAp microfibrous webs

Initial experiments were carried out to determine the optimal spinning distances as a function of sample concentrations, select the most suitable polymer solution concentrations, and define the spacing between the capillary tube and collector for PHB fiber production. Additionally, the influence of varying this parameter on the morphology of the electrospun

Table 1. Costs of the built-up electrospinning machine.

Materials	Cost (R$)
Wooden Board	60,00
Drawer Slide Rails	25,00
ATX Power Supply + Cooler + Heatsink	19,90
Flyback Transformer BSC25	40,00
Breadboard	15,00
LCD Display	10,90
Arduino Uno R3	48,90
Stepper Motor 28ybt-48 + Drive	20,90
Nylon Billet (55mm x 500mm)	52,32
Vise (Acme Thread)	45,45
U Metal Clamp 1 1/4	4,00
Steel Round Bar 6mm	5,00
Stainless Steel Tube 2" x 250mm	13,35
9V DC Motor	7,00
Others (wires, jumpers, resistors, capacitors, syringes, needles, and screws)	33,45
Labor	450,00
Total	**851,17**

Figure 1. The constructed electrospinning machine. a) Schematic diagram of the electrospinning machine; b) The built prototype of the electrospinning machine.

microfibrous webs was analyzed. Distances of 200, 250, and 300 mm from the capillary tube (with an internal diameter of 0.80 mm) to the rotating collector were tested, with the collector speed set at 580 rpm. For each of these distances, fibers were produced using solutions with concentrations of 10.0%, 12.5%, 15.0%, 17.5%, and 20.0% (m/m). The flow rate, set in the Controlled Injection System (CIS), and used for all microfibrous webs produced in this step, was 1.64 mL/h. The room temperature and humidity were maintained at 27 °C and 65%, respectively. The produced samples were designated according to the following standard: AXXXYYY. In this nomenclature, "A" represents the abbreviation of the word "Sample" in Portuguese, while "XXX" and "YYY" correspond to digits signifying the solution concentration and the distance between the capillary tube and the rotating collector, respectively.

Initial tests revealed that for distances up to 200 mm, there was ineffective solvent evaporation during spinning, resulting in the production of plastic films instead of microfibrous webs. Conversely, distances approaching 300 mm occasionally caused the electrospun jet to deviate significantly from the direction of the rotating collector. The optimal concentration/distance combination was determined to be 15.0% (m/m) at a distance of 250 mm. Consequently, these values were held constant for the analysis of the effects of varying parameters on the produced microfibrous webs, including

drum rotating speed (290 and 580 rpm), solution flow rate (2.45 and 3.27 mL/h), and internal diameter of the capillary tube (0.80 and 1.20 mm). The voltage applied during fiber production remained constant at 20 kV.

During the production process, it was determined that among all the parameter combinations assessed, the following configuration demonstrated enhanced processability and yielded superior qualitative results for the production of pure PHB fibers: a 250 mm distance between the capillary tube and the rotating collector, a collector speed set at 580 rpm, a solution flow rate of 2.45 mL/h, an internal diameter of the capillary tube measuring 0.80 mm, and an applied voltage of 20 kV. Consequently, this configuration was adopted for the production of PHB/HAp microfibrous webs. The production of PHB/HAp microfibrous webs maintained a PHB concentration of 15.0% (m/m) and an HAp concentration of 2% (m/m). Environmental conditions during production were within a temperature range of 26.0°C to 28.5°C and a humidity range of 30% to 60%.

2.4.2. Structural characterization

Fourier Transform Infrared Spectroscopy (FTIR) was employed to characterize both the PHB and the hydroxyapatite produced. For the analysis, the samples were blended with KBr, and pellets were prepared using a press before being subjected to the FTIR technique.
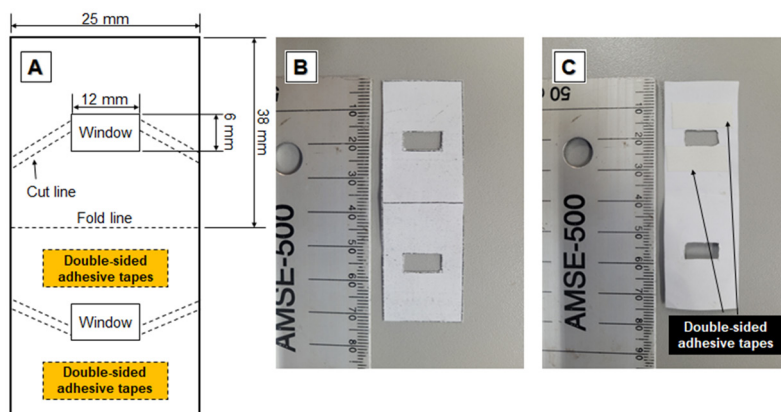
Figure 2. Template used in tensile tests: a) Schematic design of the template for sample accommodation; b) Front view of the template; c) Back view of the template where the microfibrous webs are accommodated.

The measurements were carried out over a wavelength range between 4000 and 500 cm^{-1}, by averaging 64 scans of each spectrum with a resolution on 1 cm^{-1}. The acquired data were compared with literature values for PHB and HAp. The spectrometer utilized in this analysis was the IRPrestige-21 by Shimadzu.

The Tescan Vega3 XMU scanning electron microscope, operated at an accelerating voltage of 10 kV, was utilized for imaging the microfibrous webs and observing their morphology. Prior to microscopy, all samples underwent a gold coating process using the Quorum Q150R ES Metallizer.

The micrograph was analyzed using the DiameterJ 1.018 plugin within the ImageJ 1.51 software. Scanning electron microscope images were segmented and processed for the purpose of measuring the average fiber diameter, as well as assessing the sample's porosity and fiber alignment.

2.4.3. Tensile testing

The fiber tensile tests were carried out using the EMIC DL 10000 universal testing machine. Data acquisition was performed using TESC 3.04 software, and a 500 N load cell was utilized in the universal machine. All tests were carried out at a displacement rate of 1 mm/min, following the methodology described by Boakye et al.[43]. Each sample underwent five tests. To secure the microfibrous webs, double-sided adhesive tapes were employed. Templates were used to centrally position the microfibrous webs within the template openings, which were created by printing and precise cutting. After securing the templates in the grips of the testing machine, the lateral regions were trimmed along the cutting lines, and the tests commenced. For reference, Figure 2 illustrates the template model used along with its dimensions.

3. Results and Discussion

3.1. Characterization of raw materials

Fourier Transform Infrared Spectroscopy (FTIR) was employed to characterize PHB both before and after electrospinning to assess potential structural changes.
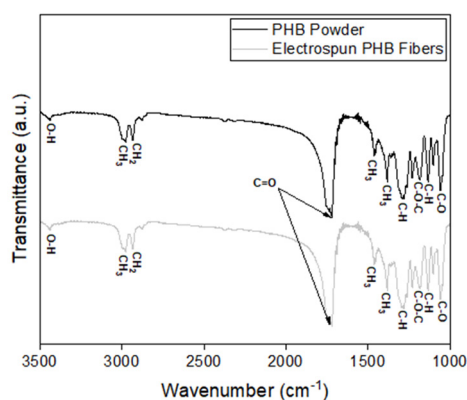
Figure 3. FTIR spectra were obtained for PHB samples in two different states: PHB powder before electrospinning and electrospun PHB fibers.

Figure 3 presents the FTIR spectrum for PHB. Characteristic PHB bands are evident in both the spectrum of PHB powder and the PHB fibers obtained through the electrospinning process, as documented in previous studies by Barbosa[44], El-Hadi et al.[45], and Furukawa et al.[46]. The identified spectral bands were as follows: 3435 cm^{-1} for O-H stretching; 2972 cm^{-1} for C-H stretching; 1726 cm^{-1} for C=O stretching; 1460 and 1382 cm^{-1} for asymmetric and symmetric CH$_3$ deformations, respectively; 1286 cm^{-1} for C-H deformation; 1282 and 1226 cm^{-1} for the stretching vibrations of C-O-C; 1176 and 1106 cm^{-1} for C-O-C stretching; 1131 cm^{-1} for CH$_3$ rocking; and 1054 cm^{-1} for C-O stretching.
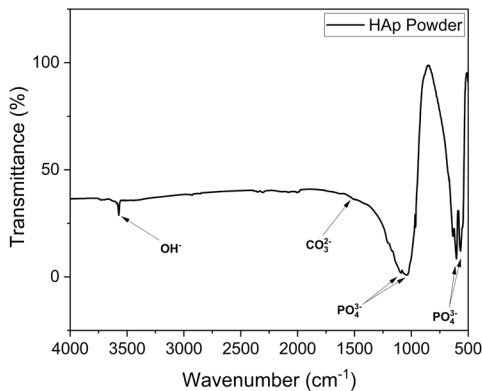
The hydroxyapatite produced through wet precipitation underwent Fourier Transform Infrared Spectroscopy (FTIR) analysis to characterize and identify its functional groups. The observed spectral bands were as follows: 3570 cm^{-1} for (-OH) groups; 1650 cm^{-1} for (CO$_3^{2-}$) groups; 1036 cm^{-1} and 1095 cm^{-1} (v_3), as well as 568 cm^{-1} and 600 cm^{-1} (v_4), which are indicative of the (PO$_4^{3-}$) ions. The FTIR spectrum obtained for HAp is presented in Figure 4, where the characteristic bands for hydroxyapatite are observed as shown in Ślósarczyk et al.[47] and Rehman and Bonfield[48].

3.2. PHB fiber production and analisys

3.2.1. Microstructural characterization of the microfibrous webs

At the outset, microfibrous webs were fabricated by systematically adjusting both the polymer concentration and the distance between the capillary tube and the collector to determine the optimal configuration for subsequent tests. Consequently, microfibrous webs were produced with variations in distance, spanning from 200 to 300 mm, and concentrations ranging between 10% and 20% (m/m). Micrographs of these samples, captured using scanning electron microscopy, are presented in Figures 5 and 6, illustrating different concentrations of the polymer solution and varying distances between the capillary tube and the rotating collector, respectively. The fibers exhibit a low surface roughness, and their diameters display uniformity in size.

The average diameters of the fibers produced in this work are presented in Tables 2 and 3. In Table 2, it is observed that as the solution concentration increased for a fixed distance,
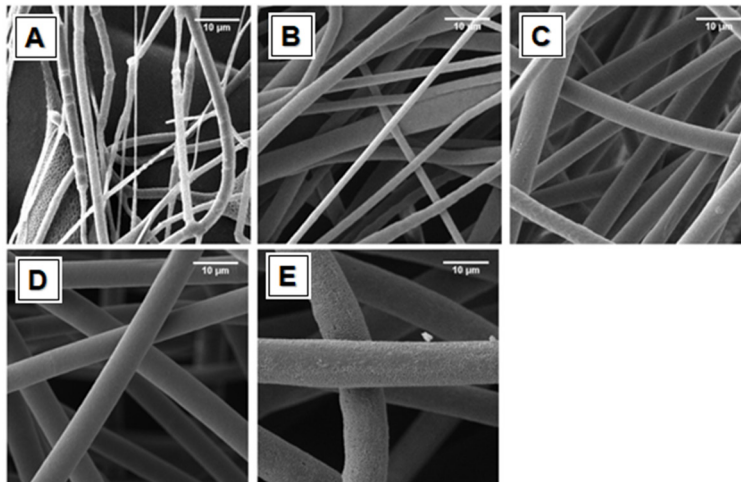
there was also an increase in the average diameter of the fibers produced. This effect of solution concentration at a constant distance between the capillary tube and rotating collector is consistent with the findings of Sukigara et al.[49], Bhardwaj and Kundu[50], Matabola and Moutloali[51], and Neo et al.[52]. Table 3 indicates that increasing the distance from the collector to the capillary tube resulted in an increase in fiber diameters, which is consistent with the results reported for fibers produced by Cramariuc et al.[53], Chen et al.[54], and Yördem et al.[55]. Nevertheless, previous studies, such as those by Kameoka and Craighead[56], Chowdhury and Stylios[57], and Bosworth and Downes[58], have reported decreases in average fiber diameters as the deposition distance on the rotary collector increases. However, when considering the errors associated with diameter measurements across these

Table 2. Average diameters of electrospun fibers at a fixed distance of 300 mm between the capillary tube and the collector for various concentrations.

Sample	Solution Concentration (m/m)	Distance (mm)	Average diameters (μm)
A100300	10.0%	300	2.10 ± 0.98
A125300	12.5%	300	2.91 ± 0.26
A150300	15.0%	300	4.77 ± 1.89
A175300	17.5%	300	6.29 ± 1.00
A200300	20.0%	300	9.61 ± 1.50

Table 3. Average diameters of electrospun fibers at a fixed concentration of 17.5% (m/m) for various distances.

Sample	Solution Concentration (m/m)	Distance (mm)	Average diameters (μm)
A175200	17.5%	200	5.68 ± 0.81
A175250	17.5%	250	5.74 ± 1.51
A175300	17.5%	300	6.29 ± 1.00

Figure 4. FTIR spectrum of HAp powder (produced through the wet precipitation method) after calcination at 900°C.

Figure 5. Micrographs of the PHB fibers for a fixed distance of 300 mm at the concentrations: a) 10.0%(m/m); b) 12.5%(m/m); c) 15.0%(m/m); d) 17.5%(m/m); and e) 20.0%(m/m).

studies, the range of variation remains minimal. Consequently, drawing a definitive conclusion about the relationship between wire diameters and deposition distances becomes challenging. Therefore, in this study, it can be concluded that the distance between the collector and the capillary tube had no significant effect on fiber diameters. While an analysis of the relationship between electric field voltage and deposition distances could provide further insights, such a study was not carried out due to the construction characteristics of the electrospinning machine.
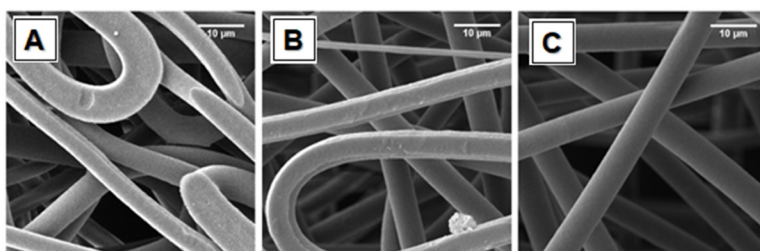
3.2.2. Porosity of PHB microfibrous webs

The percentage of porosity exhibited by the fiber assembly in each sample under different concentrations and at various distances between the capillary tube and rotary collector can be observed in Tables 4 and 5, respectively. Porosity indicates the density of fibers produced in the microfibrous webs. Thus, lower porosity means higher fiber density. Examining Table 4, we can observe that as the solution concentration increases, the porosity of the microfibrous webs decreases. The observed results suggest an increase in fiber density in the produced samples. Specifically, concerning the fixed distance between the capillary tube and the rotating collector, the decrease in porosity is directly correlated with a higher quantity of PHB in the solution, indicating a more substantial amount of polymer being electrospun. It's worth

noting that the 17.5% (m/m) sample did not conform to this observed pattern. Regarding the relationship between the porosity of PHB microfibrous webs and the distance between the capillary tube and the rotating collector, no significant influence of this parameter was noted. These findings are presented in Table 5.

### 3.2.3. Tensile characterization of PHB microfibrous webs

All the PHB microfibrous webs were tested until the complete rupture of all strands. A common characteristic among the tested samples was low elongation, indicating low ductility. Figure 7 illustrates the tensile test performed, and Table 6 presents the tensile strength and Young's modulus values of the tested fibers. It is evident that neither the tensile strength nor Young's modulus exhibited a noticeable trend or significant influence with variations in solution concentration and the distance between the rotary collector and capillary tube, consistent with prior findings by Asvar et al.[59] This is suspected to be a consequence of the pronounced non-alignment exhibited by the electrospun fibers. The low rotation speed of the drum collector used in the experiments (580 rpm) induces fiber misalignment. Due to their different angles and subsequent rotation while attempting to align with the loading direction during tensile tests, the fibers experience mechanical failure, breaking at the junctions and cohesion points between them. Thus, no significant conclusions regarding the effect of varying solution concentration and the distance between the rotary collector and capillary tube on mechanical properties could be observed[60-62].

However, by fixing the concentration at 20.0% (m/m) and varying only the distances, it was possible to evaluate the effect of changing the distance between the capillary tube and the collector on the stress-strain curves in Figure 8a. Similarly, it was possible to assess the impact of the concentration of the polymer solution by setting the distance at 250 mm and varying the concentration, as shown in Figure 8b.

By analyzing Figure 8, one can observe the fragility of PHB when subjected to mechanical stress, as also emphasized by

Table 4. Porosity of microfibrous webs for a fixed distance of 300 mm between the capillary tube and collector and varying concentrations.

Sample	Solution Concentration (m/m)	Distance (mm)	Porosity (%)
A100300	10.0%	300	48.02
A125300	12.5%	300	33.64
A150300	15.0%	300	29.22
A175300	17.5%	300	32.08
A200300	20.0%	300	20.13

Table 5. Porosity of microfibrous webs for samples with a fixed concentration of 17.5% (m/m) at different distances.

Sample	Solution Concentration (m/m)	Distance (mm)	Porosity (%)	Average diameters of electrospun fibers (μm)
A175200	17.5%	200	31.21	5.68 ± 0.81
A175250	17.5%	250	37.34	5.74 ± 1.51
A175300	17.5%	300	32.08	6.29 ± 1.00

Figure 6. Micrographs of the PHB fibers for a fixed concentration of 17.5% (m/m) at distances: a) 200 mm, b) 250 mm, and c) 300 mm.

Table 6. Tensile properties of PHB microfibrous webs.

| Sample	Solution Concentration (m/m)	Distance (mm)	Tensile Strength (MPa)	Young's Modulus (MPa)	Elongation at break (%)
A150200	15.0%	200	0.90 ± 0.14	6.90 ± 0.83	32.56 ± 15.47
A150250	15.0%	250	0.83 ± 0.08	5.23 ± 0.14	63.56 ± 33.48
A150300	15.0%	300	1.04 ± 0.16	9.25 ± 0.37	64.30 ± 26.13
A175200	17.5%	200	0.92 ± 0.13	7.95 ± 0.87	95.55 ± 46.03
A175250	17.5%	250	0.74 ± 0.05	11.87 ± 0.77	89.77 ± 42.88
A175300	17.5%	300	0.89 ± 0.13	4.90 ± 0.62	95.53 ± 23.38
A200200	20.0%	200	0.97 ± 0.13	10.50 ± 0.99	84.21 ± 16.83
A200250	20.0%	250	0.82 ± 0.09	3.91 ± 0.69	89.70 ± 31.87
A200300	20.0%	300	0.74 ± 0.03	14.47 ± 0.22	31.39 ± 11.38
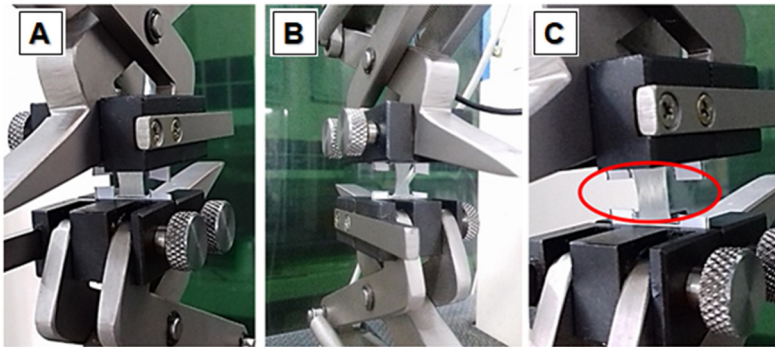
Figure 7. Tensile test performed on the electrospun PHB microfibrous webs. a) Microfibrous webs positioned before the start of the test; b) Behavior of the microfibrous webs during the test; and c) Rupture.

Arrieta et al.[63] and Ding et al.[64]. In Figure 8a, it is evident that, for a fixed solution concentration, an increase in the distance between the capillary tube and the rotating collector leads to a higher maximum stress supported by the samples. This behavior can be attributed to the decrease in fiber diameter with an increasing distance between the capillary tube and the collector. As the wire diameters become thinner, there is a more significant alignment of the molecular chains within the fibers, resulting in increased crystallinity[65]. Consequently, this molecular alignment provides enhanced resistance to tensile forces. The observed increase in tensile strength can also be attributed to the improved alignment of lamellae and fibrillar structures. These fibrillar structures exhibit a high degree of molecular orientation, as suggested by Kameoka and Craighead[56] and Baji et al.[66]. Figure 8b illustrates the impact of polymer solution concentration. As the concentration of the solution rises, there is a reduction in the ultimate tensile strength. Solutions with higher concentrations tend to produce wires with larger diameters, a phenomenon also noted in the study by Bhardwaj and Kundu[50]. Larger average fiber diameters correspond to lower tensile strength, as elucidated by Baji et al.[66].

3.3. PHB/HAP fiber production and analisys

3.3.1. Characterization of PHB/HAp microfibrous webs

The tensile strength results are presented in Table 7. It can be observed that the inclusion of hydroxyapatite
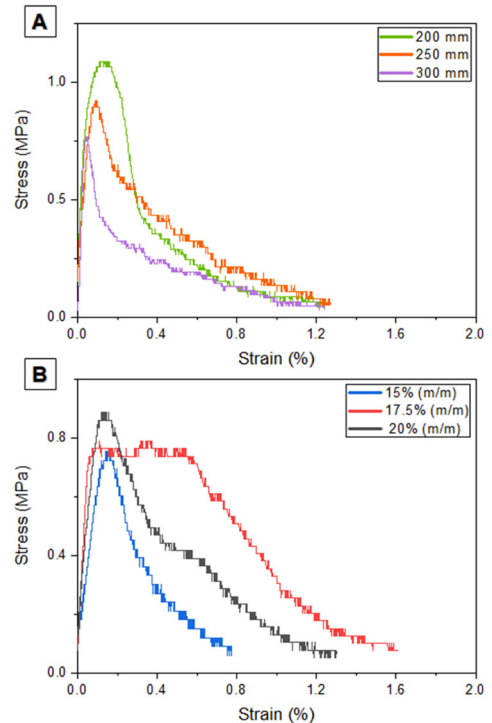
Figure 8. a) - Stress-strain curves for a 20% (m/m) sample at different distances from the collector; b) Stress-strain curves for a sample at a fixed distance of 250 mm at different concentrations.
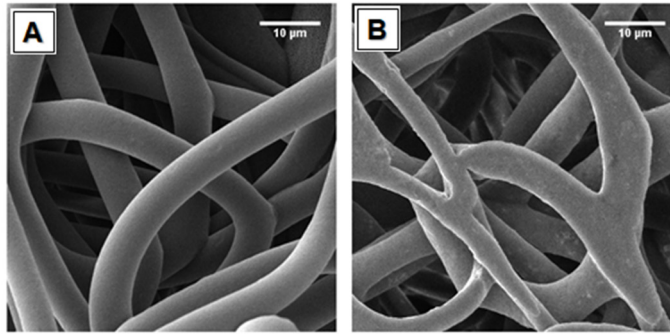
Figure 9. Micrographs of PHB fibers: a) Pure PHB fibers (15.0% m/m) and b) PHB/HAp fibers (PHB 15.0% (m/m) / 2% (m/m) HAp).

particles in the PHB fibers significantly increased both the tensile strength and Young's modulus. This enhancement is attributed to favorable interactions between the polymeric matrix and the bioceramic, which is uniformly distributed within the fibers. This characteristic acts as a filler, facilitating the efficient transfer of tensile load from the polymer to the HAp, in agreement with the findings of Ramier et al.[67].

The PHB/HAp microfibrous webs exhibited a tensile strength of 1.23 MPa, representing a 112.06% increase compared to microfibrous webs produced under the same parameters but without the addition of bioceramic. This demonstrates the excellent potential of HAp as a reinforcement for PHB in the construction of scaffolds for bone tissue engineering. Applications such as bone graft manufacturing become more viable with this enhancement. The properties of the fibers developed in this research closely resemble those reported by Chen et al.[34], who utilized similar fibers for bone graft applications. The utilization of PHB/HAp fibers for bone regeneration is also widely advocated in the studies of Guan et al.[68], Wang et al.[69], Ye et al.[70], and Doyle et al.[71].

3.3.2. Microstructural characterization of PHB/HAp microfibrous webs

The microstructure morphologies of the PHB/HAp fibers compared to the pure PHB fibers can be seen in Figure 9. Electrospinning was successful, resulting in the formation of long, continuous fibers for both microfibrous webs. The pure PHB meshes in Figure 9a appear smoother and more uniform. In contrast, the PHB/HAp meshes in Figure 9b exhibit a rougher surface. This rougher surface is attributed to the aggregation of hydroxyapatite particles in distinct regions of the fiber surface, as noted by Guan et al.[68].

The comparison of the average diameters of PHB and PHB/HAp fibers is presented in Table 8. It is evident that the average fiber diameter tends to decrease with the addition of hydroxyapatite to the polymer solution. This phenomenon can be attributed to the increased conductivity of the PHB/HAp solution compared to the PHB solution, resulting from the presence of calcium and phosphate ions from the bioceramic. Elevated conductivity in the solution corresponds to a higher capacity for electrical charge, leading to greater

Table 7. Mechanical properties comparison of PHB and PHB/HAp microfibrous webs.

Sample	Tensile Strength (MPa)	Young's Modulus (MPa)
PHB 15.0% (m/m)	0.58 ± 0.07	4.13 ± 0.90
PHB 15.0% (m/m)/ 2% HAp (m/m)	1.23 ± 0.22	13.70 ± 2.94

Table 8. Average diameters presented by PHB and PHB/HAp fibers.

Sample	Average diameters of electrospun fibers (μm)
PHB 15.0% (m/m)	7.39 ± 0.70
PHB 15.0% (m/m) / 2% HAp (m/m)	6.00 ± 0.04

Table 9. Porosity presented by PHB and PHB/HAp microfibrous webs.

Sample	Porosity (%)
PHB 15.0% (m/m)	58.72
PHB 15.0% (m/m) / 2% HAp (m/m)	54.47

stretching forces and, consequently, smaller fiber diameters, as reported by Ramier et al.[67].

3.3.3. The porosity of PHB/HAp microfibrous webs

The porosity of both PHB and PHB/HAp microfibrous webs is presented in Table 9. Interestingly, the addition of hydroxyapatite to the solution resulted in a slight decrease in the fabric's fiber density, contrary to our expectations. Typically, the reduction in average fiber diameters due to the addition of HAp leads to lower fabric porosity, as described by Chen et al.[34]. Nonetheless, the microfibrous webs developed in this study exhibited a consistently high level of porosity in the produced microfibrous webs, averaging approximately 60% for all fiber samples. This high porosity is advantageous for facilitating adhesion, infiltration, and cell growth, particularly in the context of bone and cartilage tissue regeneration. It is worth noting that greater porosity in electrospun microfibrous webs has been linked to increased cell infiltration, as demonstrated by Thorvaldsson et al.[72].

4. Conclusions

The constructed electrospinning system demonstrated its efficiency as all PHB and PHB/HAp solutions used produced satisfactory electrospun fibers, facilitating the fabrication of scaffolds. These developed microfibrous webs allowed for the investigation of how electrospinning parameters influence their morphology.

The variation in electrospinning parameters significantly influenced the properties of the electrospun fibers. It was observed that the porosity of the microfibrous webs decreased with increasing concentration, indicating a higher fiber density in the produced samples.

Moreover, an increase in the concentration of the polymer solutions led to a decrease in the mechanical strength of the microfibrous webs, attributed to the production of fibers with larger diameters when using solutions with high concentrations. The average diameter of the pure PHB fibers ranged from 2.10 to 9.61 μm.

The addition of hydroxyapatite increased the tensile strength by 112.06% compared to pure PHB microfibrous webs. The average diameter of the PHB/HAp fibers was smaller than that of the PHB fibers. The porosity of the microfibrous webs decreased when HAp was incorporated into the fiber production.

5. Acknowledgments

6. References

1. Agarwal S, Greiner A, Wendorff JH. Functional materials by electrospinning of polymers. Prog Polym Sci. 2013;38(6):963-91.

2. Al-Husaini IS, Yusoff ARM, Lau WJ, Ismail AF, Al-Abri MZ, Al-Ghafri BN, et al. Fabrication of polyethersulfone electrospun nanofibrous membranes incorporated with hydrous manganese dioxide for enhanced ultrafiltration of oily solution. Separ Purif Tech. 2019;212:205-14.

3. Zhu Y, Yang D, Li J, Yue Z, Zhou J, Wang X. The preparation of ultrathin and porous electrospinning membranes of HKUST-1/PLA with good antibacterial and filtration performances. J Porous Mater. 2023;30(3):1011-9.

4. Ren J, Liu T, An X, Wu F, Xie C. Preparation and property of antibacterial filter membrane by coaxial electro-spraying/electrospinning technology. J Appl Polym Sci. 2024;141(4):e54847.

5. Zaborowska M, Smok W, Tański T. Electrospun niobium oxide 1D nanostructures and their applications in textile industry wastewater treatment. Bull Pol Acad Sci Tech Sci. 2023;71(2):e144941.

6. Metwally BS, Zayed AM, Rashed SA, El-Sheikh MN, Hamouda AS. Sustainable Nano-nonwoven fabric production from recycled polyamide 6 waste via electrospinning: controlling characteristics and comprehensive analytical study. Adv Mater Technol. 2023;8(18):2300509.

7. Bili O, Elkalaaoui K, Boukhriss A, Ait Chaoui M, Majid S, El Kouali M, et al. Novel lightweight and flexible functional textile based on PVDF and [Im, PF6] developed via the electrospinning technique. Prog Org Coat. 2024;186:108019.

8. Zhang Q, Lin S, Wang Z, Li J, Xiao J. Lipase-interfacial catalytic systems based on hybrid membranes constructed via electrospinning and gelation. Lebensm Wiss Technol. 2023;183:114956.

9. Jiao Y, Jing C, Wang Y, Yao F, Ye G, Wang X, et al. Electrospinning synthesis of Co3O4 porous nanofiber monolithic catalysts for the room-temperature indoor catalytic oxidation of formaldehyde at low concentrations. Appl Surf Sci. 2023;639:158215.

10. He F, Wang Y, Liu J, Yao X. One-dimensional carbon based nanoreactor fabrication by electrospinning for sustainable catalysis. Exploration. 2023;3(3):20220164.

11. Santos AL, Duarte MAT, Pezzin SH, Silva L, Domingues JA. Preparation of porous poly (lactic acid) fibers by medium field electrospinning for tissue engineering applications. Mater Res. 2020;23(2):e20190468.

12. Chen K, Li Y, Li Y, Pan W, Tan G. Silk fibroin combined with electrospinning as a promising strategy for tissue regeneration. Macromol Biosci. 2023;23(2):2200380.

13. Armenio L, Fare' S, Draghi L. A direct-writing electrospinning system for designing complex architectures in tissue engineering. Biomed Phys Eng Express. 2024;10(2):027001.

14. Juncos Bombin AD, Dunne NJ, McCarthy HO. Electrospinning of natural polymers for the production of nanofibres for wound healing applications. Mater Sci Eng C. 2020;114:110994.

15. Wen Z, Chen Y, Liao P, Wang F, Zeng W, Liu S, et al. In situ precision cell electrospinning as an efficient stem cell delivery approach for cutaneous wound healing. Adv Healthc Mater. 2023;12(26):2300970.

16. Li J, Zhang S, He C, Ling J. Electrospun fibers based anisotropic silk fibroin film with photodynamic antibacterial therapy for S. aureus infected wound healing. Int J Biol Macromol. 2024;254:127685.

17. Tabakoglu S, Kołbuk D, Sajkiewicz P. Multifluid electrospinning for multi-drug delivery systems: pros and cons, challenges, and future directions. Biomater Sci. 2022;11(1):37-61.

18. Ghosal K, Augustine R, Zaszczynska A, Barman M, Jain A, Hasan A, et al. Novel drug delivery systems based on triaxial electrospinning based nanofibers. React Funct Polym. 2021;163:104895.

19. Bulbul YE, Uygun Oksuz A. Cold atmospheric plasma modified polycaprolactone solution prior to electrospinning: a novel approach for improving quercetin-loaded nanofiber drug delivery systems. Int J Pharm. 2024;651:123789.

20. Dognani G, Cabrera FC, Cavalcante DGSM, Boina RF, Job AE, Agostini DLS. nanofibrous membranes for low-concentration CrVI adsorption: kinetic, thermodynamic and the influence on ZFL cells viability. Mater Res. 2021;24(Suppl 1):e20210006.

21. Capilli G, Sartori DR, Gonzalez MC, Laurenti E, Minero C, Calza P. Non-purified commercial multiwalled carbon nanotubes supported on electrospun polyacrylonitrile@polypyrrole nanofibers as photocatalysts for water decontamination. RSC Adv. 2021;11(17):9911-20.

22. Cao W, Zhang M, Ma W, Huang C. Multifunctional electrospun nanofibrous membrane: an effective method for water purification. Separ Purif Tech. 2023;327:124952.

23. El-Hadi A, Al-Jabri F. Influence of electrospinning parameters on fiber diameter and mechanical properties of poly(3-Hydroxybutyrate) (PHB) and polyanilines (PANI) blends. Polymers. 2016;8(3):97.

24. Mohammadalipour M, Asadolahi M, Mohammadalipour Z, Behzad T, Karbasi S. Plasma surface modification of electrospun polyhydroxybutyrate (PHB) nanofibers to investigate their performance in bone tissue engineering. Int J Biol Macromol. 2023;230:123167.

25. Olkhov AA, Tyubaeva PM, Zernova YN, Markin VS, Kosenko R, Filatova AG, et al. The Influence of technological factors and polar molecules on the structure of fibrillar matrices based on ultrafine Poly-3-hydroxybutyrate fibers obtained via electrospinning. Technologies. 2023;11(5):118.

26. Sadat-Shojai M, Khorasani MT, Jamshidi A, Irani S. Nano-hydroxyapatite reinforced polyhydroxybutyrate composites: a

comprehensive study on the structural and in vitro biological properties. Mater Sci Eng C. 2013;33(5):2776-87.

27. Tomer P, Shroti GK, Mohapatra S, Ghosh D, Jaiswal S, Garg D, et al. Fabrication of HA nano-crystal reinforced PHAs based composites for orthopedic fracture-fixing accessories using sustainable resources. Environ Dev Sustain. 2023. In press.

28. Kopf S, Åkesson D, Hakkarainen M, Skrifvars M. Effect of hydroxyapatite particle morphology on as-spun poly(3-hydroxybutyrate-co-3-hydroxyvalerate)/hydroxyapatite composite fibers. Results in Materials. 2023;20:100465.

29. Sadat-Shojai M. Electrospun polyhydroxybutyrate/hydroxyapatite nanohybrids: microstructure and bone cell response. J Mater Sci Technol. 2016;32(10):1013-20.

30. Venkatesan J, Kim SK. Nano-hydroxyapatite composite biomaterials for bone tissue engineering: a review. J Biomed Nanotechnol. 2014;10(10):3124-40.

31. Shi H, Zhou Z, Li W, Fan Y, Li Z, Wei J. Hydroxyapatite based materials for bone tissue engineering: a brief and comprehensive introduction. Crystals. 2021;11(2):149.

32. Verma R, Mishra SR, Gadore V, Ahmaruzzaman M. Hydroxyapatite-based composites: excellent materials for environmental remediation and biomedical applications. Adv Colloid Interface Sci. 2023;315:102890.

33. Oni OP, Hu Y, Tang S, Yan H, Zeng H, Wang H, et al. Syntheses and applications of mesoporous hydroxyapatite: a review. Mater Chem Front. 2022;7(1):9-43.

34. Chen Z, Song Y, Zhang J, Liu W, Cui J, Li H, et al. Laminated electrospun nHA/PHB-composite scaffolds mimicking bone extracellular matrix for bone tissue engineering. Mater Sci Eng C. 2017;72:341-51.

35. Du JH, Ren LY, Zhang B. Preparation of PHB/PLLA/n-HA composite ultrafine fibers via electrospinning. Adv Mat Res. 2013;821–822:179-83.

36. Krucińska I, Żywicka B, Komisarczyk A, Szymonowicz M, Kowalska S, Zaczyńska E, et al. Biological properties of low-toxicity PLGA and PLGA/PHB fibrous nanocomposite implants for osseous tissue regeneration. Part I: evaluation of potential biotoxicity. Molecules. 2017;22(12):2092.

37. Krucińska I, Chrzanowska O, Boguń M, Kowalczuk M, Dobrzyński P. Fabrication of PLGA/HAp and PLGA/PHB/HAp fibrous nanocomposite materials for osseous tissue regeneration. AUTEX Res J. 2014;14(2):95-110.

38. Yusro M, Kadarisman K. Development of low-cost electrospinning to fabricate structured nanofiber for biomedical designs with manageable flowrate and voltage. Indones J Electron Electromed Eng Med Inf. 2022;4(3):123-30.

39. Abu Owida H, Al-haj Moh'd B, Al Takrouri M. Designing an integrated low-cost electrospinning device for nanofibrous scaffold fabrication. HardwareX. 2022;11:e00250.

40. Wijayanti ID, Saputra AK, Ibrahim F, Rasyida A, Suwarta P, Sidharta I. An ultra-low-cost and adjustable in-house electrospinning machine to produce PVA nanofiber. HardwareX. 2022;11:e00315.

41. Velasco Barraza RD, Álvarez Suarez AS, Villarreal Gómez LJ, Paz González JA, Iglesias AL, Vera Graziano R. Designing a low cost electrospinning device for practical learning in a bioengineering biomaterials course. Rev Mex Ing Biomed. 2016;37:27.

42. Álvares TV S. Caracterização de cerâmicas densas de hidroxiapatita produzidas a partir do gesso [dissertação]. Juazeiro: Universidade Federal do Vale do São Francisco; 2012.

43. Boakye M, Rijal N, Adhikari U, Bhattarai N. Fabrication and characterization of electrospun PCL-MgO-keratin-based composite nanofibers for biomedical applications. Materials. 2015;8(7):4080-95.

44. Barbosa AA. Estudo da conversão química de compósitos a base de gesso em hidroxiapatita [dissertação]. Juazeiro: Universidade Federal do Vale do São Francisco; 2012.

45. El-Hadi A, Schnabel R, Straube E, Müller G, Riemschneider M. Effect of melt processing on crystallization behavior and rheology of poly(3-hydroxybutyrate) (PHB) and its blends. Macromol Mater Eng. 2002;287(5):363.

46. Furukawa T, Sato H, Murakami R, Zhang J, Duan YX, Noda I, et al. Structure, dispersibility, and crystallinity of poly(hydroxybutyrate)/poly(l-lactic acid) blends studied by FT-IR microspectroscopy and differential scanning calorimetry. Macromolecules. 2005;38(15):6445-54.

47. Ślósarczyk A, Paszkiewicz Z, Paluszkiewicz C. FTIR and XRD evaluation of carbonated hydroxyapatite powders synthesized by wet methods. J Mol Struct. 2005;744–747:657-61.

48. Rehman I, Bonfield W. Characterization of hydroxyapatite and carbonated apatite by photo acoustic FTIR spectroscopy. J Mater Sci Mater Med. 1997;8(1):1-4.

49. Sukigara S, Gandhi M, Ayutsede J, Micklus M, Ko F. Regeneration of Bombyx mori silk by electrospinning. Part 1: processing parameters and geometric properties. Polymer. 2003;44(19):5721-7.

50. Bhardwaj N, Kundu SC. Electrospinning: a fascinating fiber fabrication technique. Biotechnol Adv. 2010;28(3):325-47.

51. Matabola KP, Moutloali RM. The influence of electrospinning parameters on the morphology and diameter of poly(vinyledene fluoride) nanofibers- effect of sodium chloride. J Mater Sci. 2013;48(16):5475-82.

52. Neo YP, Ray S, Easteal AJ, Nikolaidis MG, Quek SY. Influence of solution and processing parameters towards the fabrication of electrospun zein fibers with sub-micron diameter. J Food Eng. 2012;109(4):645-51.

53. Cramariuc B, Cramariuc R, Scarlet R, Manea LR, Lupu IG, Cramariuc O. Fiber diameter in electrospinning process. J Electrost. 2013;71(3):189-98.

54. Chen ZG, Wei B, Mo XM, Cui FZ. Diameter control of electrospun chitosan-collagen fibers. J Polym Sci, B, Polym Phys. 2009;47(19):1949-55.

55. Yördem OS, Papila M, Menceloğlu YZ. Effects of electrospinning parameters on polyacrylonitrile nanofiber diameter: an investigation by response surface methodology. Mater Des. 2008;29(1):34-44.

56. Kameoka J, Craighead HG. Fabrication of oriented polymeric nanofibers on planar surfaces by electrospinning. Appl Phys Lett. 2003;83(2):371-3.

57. Chowdhury M, Stylios G. Effect of experimental parameters on the morphology of electrospun nylon 6 fibres. Int J Basic Appl Sc. 2010;10:70-8.

58. Bosworth LA, Downes S. Acetone, a sustainable solvent for electrospinning poly(ε-caprolactone) fibres: effect of varying parameters and solution concentrations on fibre diameter. J Polym Environ. 2012;20(3):879-86.

59. Asvar Z, Mirzaei E, Azarpira N, Geramizadeh B, Fadaie M. Evaluation of electrospinning parameters on the tensile strength and suture retention strength of polycaprolactone nanofibrous scaffolds through surface response methodology. J Mech Behav Biomed Mater. 2017;75:369-78.

60. Tarus B, Fadel N, Al-Oufy A, El-Messiry M. Effect of polymer concentration on the morphology and mechanical characteristics of electrospun cellulose acetate and poly (vinyl chloride) nanofiber mats. Alex Eng J. 2016;55(3):2975-84.

61. Lins LC, Wianny F, Livi S, Dehay C, Duchet-Rumeau J, Gérard JF. Effect of polyvinylidene fluoride electrospun fiber orientation on neural stem cell differentiation. J Biomed Mater Res B Appl Biomater. 2017;105(8):2376-93.

62. O'Connor RA, Cahill PA, McGuinness GB. Effect of electrospinning parameters on the mechanical and morphological characteristics of small diameter PCL tissue engineered blood vessel scaffolds having distinct micro and nano fibre populations: a DOE approach. Polym Test. 2021;96:107119.

63. Arrieta MP, López J, López D, Kenny JM, Peponi L. Development of flexible materials based on plasticized electrospun PLA-PHB blends: structural, thermal, mechanical and disintegration properties. Eur Polym J. 2015;73:433-46.

64. Ding Y, Roether JA, Boccaccini AR, Schubert DW. Fabrication of electrospun poly (3-hydroxybutyrate)/poly (ε-caprolactone)/silica hybrid fibermats with and without calcium addition. Eur Polym J. 2014;55:222-34.

65. Wong SC, Baji A, Leng S. Effect of fiber diameter on tensile properties of electrospun poly(ε-caprolactone). Polymer. 2008;49(21):4713-22.

66. Baji A, Mai YW, Wong SC, Abtahi M, Chen P. Electrospinning of polymer nanofibers: effects on oriented morphology, structures and tensile properties. Compos Sci Technol. 2010;70(5):703-18.

67. Ramier J, Bouderlique T, Stoilova O, Manolova N, Rashkov I, Langlois V, et al. Biocomposite scaffolds based on electrospun poly(3-hydroxybutyrate) nanofibers and electrosprayed hydroxyapatite nanoparticles for bone tissue engineering applications. Mater Sci Eng C. 2014;38:161-9.

68. Guan D, Chen Z, Huang C, Lin Y. Attachment, proliferation and differentiation of BMSCs on gas-jet/electrospun nHAP/PHB fibrous scaffolds. Appl Surf Sci. 2008;255(2):324-7.

69. Wang YW, Wu Q, Chen GQ. Attachment, proliferation and differentiation of osteoblasts on random biopolyester poly(3-hydroxybutyrate-co-3-hydroxyhexanoate) scaffolds. Biomaterials. 2004;25(4):669-75.

70. Ye C, Hu P, Ma MX, Xiang Y, Liu RG, Shang XW. PHB/PHBHHx scaffolds and human adipose-derived stem cells for cartilage tissue engineering. Biomaterials. 2009;30(26):4401-6.

71. Doyle C, Tanner ET, Bonfield W. In vitro and in vivo evaluation of polyhydroxybutyrate and of polyhydroxybutyrate reinforced with hydroxyapatite. Biomaterials. 1991;12(9):841-7.

72. Thorvaldsson A, Stenhamre H, Gatenholm P, Walkenström P. Electrospinning of highly porous scaffolds for cartilage regeneration. Biomacromolecules. 2008;9(3):1044-9.